*Article*

# Interfacial Behavior of Slag, Fly Ash, and Red Mud-Based Geopolymer Mortar with Concrete Substrate: Mechanical Properties and Microstructure

Qinghui Long [1], Yufei Zhao [2,*], Benben Zhang [3,*], Huichen Yang [2], Zhengdong Luo [4], Zhengyang Li [4], Genbao Zhang [5] and Kun Liu [6]

[1] Yiyang Highway and Bridge Construction Co., Ltd., Yiyang 413000, China; yylqlongqh@163.com
[2] China Institute of Water Resources and Hydropower Research, Beijing 100041, China; yanghc@iwhr.com
[3] School of Transportation, Southeast University, Nanjing 211189, China
[4] College of Civil Engineering, Xiangtan University, Xiangtan 411105, China; luozhengdong0425@163.com (Z.L.); 17700238543@163.com (Z.L.)
[5] College of Civil Engineering, Hunan City University, Yiyang 413000, China; genbao@hncu.edu.cn
[6] Hunan Zhitong Expressway Construction and Development Co., Ltd., Changsha 410026, China; ztgsluik@163.com
[*] Correspondence: zhaoyf@iwhr.com (Y.Z.); 230238946@seu.edu.cn (B.Z.)

**Abstract:** Geopolymer, as a new type of solid waste-based inorganic cementitious material, exhibits outstanding behavior in terms of physical and chemical performance, macromechanical properties, long-lasting stability, and features potential application development tendency in the field of repair and reinforcement of existing concrete structures. This paper investigated the interfacial behavior of geopolymer mortar with OPC concrete substrate under different slag, fly ash and red mud mixing proportions, while cement mortar was used as a control group for the research. The interfacial bonding properties of the geopolymer mortar to the OPC concrete substrate were elaborated by carrying out split tensile test, double-sided shear test, and three-point bending test. Scanning electron microscopy (SEM) and X-ray diffraction (XRD) were employed to further analyze the microstructural characteristics and physical phase components of the interfacial transition zone between the geopolymer mortar and the OPC concrete substrate. The results indicated that the compressive strength of slag-fly ash-red mud-based geopolymer mortar under different mixing ratio conditions was consistently superior to that of cement mortar, where the optimum mixing ratio for the geopolymer mortar was S33F33R33. Overall, the interfacial bonding properties of the geopolymer mortar to the OPC concrete substrate gradually increased with the increment of the slag content, however, an evolutionary trend of minor enhancement followed by a gradual reduction was observed with the growth of the fly ash and red mud content.

**Keywords:** interfacial behavior; slag; fly ash and red mud; geopolymer mortar; concrete substrate; mechanical properties

## 1. Introduction

Since its introduction, concrete has been one of the most common and widely used construction materials in the field of civil engineering, mainly but not limited to industrial and civil buildings, bridges and tunnels, road traffic and water conservancy projects and other engineering construction facilities [1–3]. As a result of adverse conditions such as human factors or the external natural environment, concrete structures suffer from different degrees of structural damage phenomena with the growth of service time, mainly including concrete protective layer peeling [4], surface cracking [5], and reinforcement corrosion [6]. This significantly reduces the concrete structure's load-bearing capacity, seriously threatening the normal use and service life of the overall structure, inevitably

increasing the risk of use and safety hazards. The deterioration of concrete structures is mainly attributed to changing and alternating loads (fatigue loading, traffic loading, overload bearing [7–9]), attack of the external environment (carbonation, chemical ion attack, wet-dry and freeze-thaw cycles [10–12]), and structural deformation (shrinkage and creep [13,14]). Therefore, it is a technical challenge for engineers in civil engineering to improve the load-bearing performance and service life of existing concrete structures through strengthening and rehabilitation measures.

The grouting repair method is widely used in the repair and strengthening of existing concrete structures because of the advantages of good reinforcement effect, high construction efficiency, economy, and adaptability [15]. Specifically, inorganic or organic repair materials are injected into the defects of existing concrete structure, through the repair materials in the process of solidification and hardening of the physical-chemical effect on the existing concrete, so as to achieve the purpose of improving the load-bearing performance and service life of the existing concrete structure. Currently, the most widely used repair materials are cement-based materials, mainly including Portland cement mortar (PCM) [16], self-compacting concrete (SCC) [17], high-performance fiber-reinforced concrete (HPFRC) [18], and ultra-high-performance concrete (UHPC) [19]. It is undeniable that cement-based materials play an important role in the field of the repair and reinforcement of existing concrete structures, mainly from their good compatibility with concrete. With the concept of green and sustainable development in human society, cement-based materials have gradually exposed various shortcomings. As an energy-intensive industry, cement inevitably exists with the disadvantages of high energy consumption, environmental pollution, and high greenhouse gas emissions, which undoubtedly increases the pressure on the ecological environment, and is therefore not conducive to sustainable human development [20]. It is reported that the cement industry releases about 7% of the total global $CO_2$ emissions from all industries [21]. Thus, from the viewpoint of eco-friendly and sustainable development, there are certain limitations and restrictions in using cement-based cementitious materials to repair and strengthen existing concrete structures.

As one of the current research hotspots in the field of civil engineering materials, geopolymer has received wide attention from researchers in view of the significant advantages of low carbon and environmental protection, low energy consumption, and high resource utilization rate of industrial solid waste [22]. In addition to this, previous studies have reported that the performance of geopolymer is not inferior to that of ordinary Portland cement in terms of mechanical properties, durability, and high temperature resistance [23,24]. Based on the results presented above, the call for replacing cement with geopolymer in civil engineering is gaining more and more response and support from researchers. Specifically, geopolymer refers to a three-dimensional network of inorganic gel material assembled from aluminum-oxygen tetrahedra and silica-oxygen tetrahedra formed by the dissolution, monomer reconstruction, and monomer condensation stages of precursor materials rich in active silica-alumina mineral components under the action of alkali activator [25]. One of the potential applications of geopolymer is the repair and reinforcement of existing concrete structures because of its high early strength and superior interfacial bonding characteristics.

The silica-aluminate mineral raw material, which is one of the variables, has a significant role in influencing the various properties of geopolymer. The raw material sources of silica-aluminate minerals are mainly but not limited to industrial solid wastes (blast furnace slag, fly ash [26,27]), natural minerals (metakaolin, calcined clay [28,29]), and nonferrous metal tailings (gold mine tailings, copper mine tailings [30,31]). Currently, the precursor raw materials of geopolymer applied relatively widely in the field of repair and reinforcement of existing concrete structures are mainly slag and fly ash, which are usually in the form of individual or composite. Laskar et al. [32] compared the performance of ultra-fine slag-based geopolymer mortar (GPM) and Portland cement mortar (PCM) for the repair of damaged full-size reinforced concrete beam via static four-point bending test. The experiment results indicated that the reinforced concrete beam repaired via PCM

indicated higher load-bearing capacity and ductility compared to PCM. Gomaa et al. [7] and Zailani et al. [33] investigated the effect of calcium content on the interfacial bonding properties of fly ash-based alkali-activated concrete (AAC) and ordinary Portland cement concrete (OPCC) via indoor mechanical tests such as diagonal shear test and pull-out test. The results showed that the interfacial bond strength between ACC and OPCC gradually enhanced with the increase in calcium content in fly ash, which was mainly attributed to the increase in the number of calcium-based hydration gel products. Wang et al. [34] further noted that the width of the interfacial transition zone (ITZ) of geopolymer repair mortar (GRM) and OPCC gradually widened with increasing calcium content in the geopolymer precursor material, resulting in a more uniform force state and better compatibility at the repair interface. In summary, it can be speculated that geopolymer mortar prepared from slag or fly ash can be applied to the repair and reinforcement of existing concrete structures with a considerable strengthening effect.

As a highly alkaline waste sludge discharged from alumina production, red mud disposed of directly in landfills without treatment not only occupies land resources and causes soil salinization but also contributes to groundwater contamination that is difficult to recover [35–37]. In addition, red mud with a large specific surface area is prone to dust generation and air pollution under open accumulation condition [38]. In response to these unfavorable factors, the comprehensive utilization of red mud is mostly in the field of construction materials, mainly being used for the preparation of concrete blocks [39], sintered bricks [40], ceramic tiles [41], and concrete admixtures [42], but the comprehensive utilization of red mud by these measures is still at a relatively low level. In order to further improve the utilization of red mud, some researchers have successfully demonstrated the feasibility and applicability of the preparation of geopolymer from red mud. The literature [43–45] has reported that red mud-based geopolymer possesses good mechanical properties, durability, and performance stability. In conclusion, the preparation of red mud into geopolymer is an effective and reasonable disposal treatment measure for bauxite residues, but few studies related to the use of red mud based geopolymer for the repair and reinforcement of existing concrete structures have been reported [46].

In view of this, this study attempted to confirm the feasibility of slag-fly ash-red mud-based geopolymer mortar (GPM) to repair and strengthen OPC concrete substrate through a series of indoor mechanical tests. Firstly, the mechanical properties of GPM prepared from different precursor raw material ratios were evaluated. Then, the mechanism of the effect of precursor raw material ratio on the interfacial bond strength between GPM and OPC concrete substrate was investigated via double-sided shear test, splitting tensile test, and three-point bending test. Finally, SEM and XRD were utilized to further analyze the microstructure and hydride phase composition of the interfacial transition zone between GPM and OPC concrete substrate.

## 2. Materials and Methods

### 2.1. Raw Materials

In this paper, slag, fly ash, and red mud were selected as composite silica-aluminate raw materials for the preparation of geopolymer. The slag belonged to ground granulated blast slag, S105 grade, provided by Gongyi Longze Water Purification Material Co., Ltd., in Henan, China, the fly ash was F class low calcium fly ash, supplied by Zhengzhou Rongchang Sheng Environmental Protection Material Co., Ltd., in Henan, China, and the red mud was the by-product of alumina extraction from bauxite via Bayer method, offered by Zhengzhou Xinyuan New Material Co., Ltd., in Henan, China. It should be mentioned that the red mud used in the experiment should first be placed in an electric drying oven at 80 °C for 12 h, then crushed in a jaw crusher for 3 min, ground in a ball mill for 30 min, and finally sieved through a 250 μm geosynthetic sieve. The cement used for the preparation of concrete substrate and cement repair mortar was P.O 42.5 grade, supplied by Xiangxiang Chengmei Cement Co., Ltd., in Hunan, China. The microscopic morphology of the raw materials used in the test is shown in Figure 1, in which the microstructures of

slag, fly ash, and red mud have different morphologies. The slag particles were mostly irregular polygonal with clear contours and rough surfaces, with some small particles piled up on the surface of large particles. The surface of fly ash particles is smooth and dense, constituted by spherical vitreous microbeads of different sizes. The structure of red mud is loose, with large porosity and the distribution of fine crystal particle agglomerates. The cement is composed of haphazardly distributed lumpy particles, with more internal pore defects and rough surfaces. The chemical composition (in oxide form) of the raw materials used in the experiment was characterized via X-ray fluorescence spectroscopy (XRF), as presented in Table 1. The coarse aggregate used for the preparation of concrete substrate was well-graded crushed stone with a maximum particle size of 10 mm and a minimum particle size of 4.75 mm; the fine aggregate was river sand with a fineness modulus of 2.49, which originated from Xiangjiang river in China. The water used for the whole experiment was tap water.
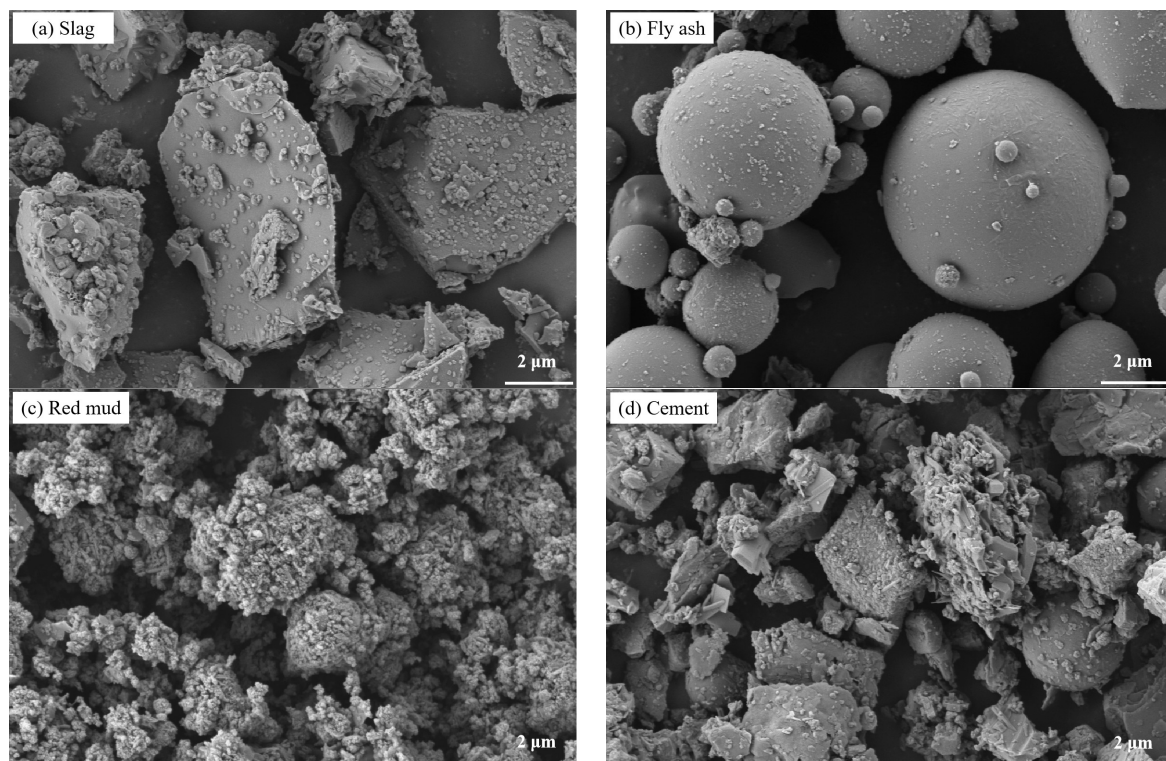


**Figure 1.** The SEM images of raw materials.

**Table 1.** The Chemical composition of raw materials (%).

| | CaO | $Al_2O_3$ | $SiO_2$ | MgO | $Fe_2O_3$ | $SO_3$ | $K_2O$ | $TiO_2$ | Others | LOI |
|---|---|---|---|---|---|---|---|---|---|---|
| Slag | 35.30 | 16.70 | 34.50 | 5.01 | 1.50 | 1.24 | - | - | 5.75 | 1.85 |
| Fly ash | 2.32 | 34.70 | 53.04 | 0.86 | 2.53 | 0.35 | 1.76 | 1.25 | 3.19 | 2.38 |
| Red mud | 1.01 | 11.06 | 25.79 | 1.01 | 53.63 | 1.17 | 1.44 | 2.02 | 2.87 | 1.96 |
| cement | 49.20 | 11.52 | 27.50 | 1.18 | 3.38 | - | - | - | 7.22 | 2.06 |

Previous studies [47,48] have consistently reported that composite alkali activator tend to be more superior to the activation of silica-aluminate raw materials than a single alkali activator, specifically to enable silica-aluminate raw materials to undergo sufficient geopolymerization reaction processes such as depolymerization and polycondensation, which makes the geopolymer reflect better mechanical characteristics and durability. In view of this, for reasons of rationality, reference, and economy, this study used sodium silicate solution and tablet sodium hydroxide to prepare a composite alkali activator

solution with a modulus of 1.2, which was consistent with the findings of related study [49], which concluded that 19.14 g of solid sodium hydroxide fragments were added per 100 g of sodium silicate solution. The sodium silicate solution exhibited an initial modulus of 3.31, a BoM of 38.5 Be, and the main chemical composition of $Na_2O$ (8.42 wt%), $SiO_2$ (27.84 wt%), and $H_2O$ (63.74 wt%). The tablet sodium hydroxide was analytically pure, with a purity greater than 98%.

### 2.2. OPC Concrete Substrate

The OPC concrete substrate was formulated with the mass ratio of coarse aggregate: fine aggregate: cement/water as 1130:664: 402:205, and its design strength grade was C30. In order to investigate the interfacial bonding properties between different concrete substrates and GPM, a split tensile test, a double-sided shear test, and a three-point bending test were carried out, as shown in Figure 2. Prior to these tests, freshly mixed concrete paste was cast into concrete substrates of different sizes and shapes, in which the mold sizes of the concrete substrates were 150 mm × 150 mm × 75 mm, 150 mm × 150 mm × 100 mm, and 100 mm × 100 mm × 350 mm, respectively. The concrete substrates were prepared by pouring the freshly stirred concrete slurry into the corresponding concrete molds in layers, followed by adequate vibration and pounding, after which the concrete surface was smoothed with a scraper and placed in a room for 1 d. After completion of the curing process, the molds were demolished and the concrete substrates were transferred to a standard curing room (temperature 22 ± 2 °C, humidity not less than 95%) for continuous curing for 28 d. In order to further exploit the mechanical interlocking effect and frictional resistance of the concrete substrate interface, and thus maximize the interfacial bonding performance between the GPM and the concrete substrate, the concrete substrate interface was roughened via mechanical grinding [50]. In view of the above expression, the roughness depth indicated via the different types of concrete substrates was regulated to 5 mm in the same way to achieve consistency in mechanical tests.
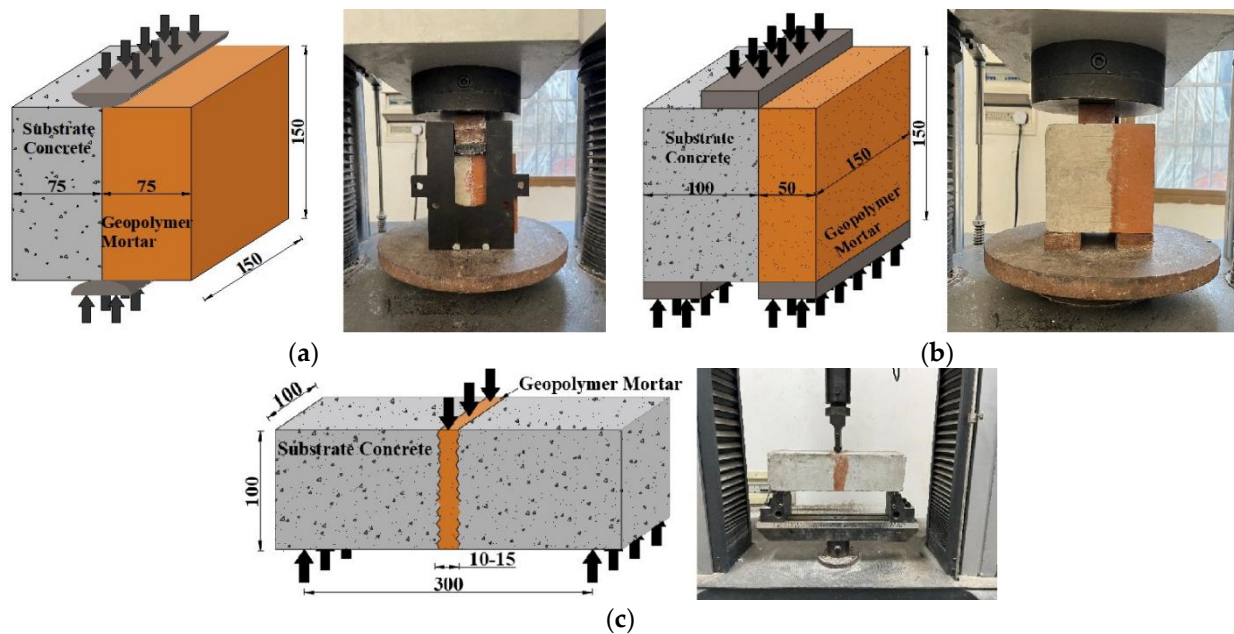


**Figure 2.** Interface bonding performance test between geopolymer mortar and concrete substrate. (**a**) Splitting tensile test, (**b**) double-sided shear test, (**c**) three-point bending test.

### 2.3. Geopolymer Mortar

The ratio scheme of the GPM is shown in Table 2. The design scheme of the GPM was to use slag, fly ash, and red mud as unit variables respectively. The remaining two types of silica-aluminate raw materials were blended in equal proportions, where the blending

amounts of slag, fly ash, and red mud were all designed to be 10%, 15%, 20%, and 33%. For example, S10F45R45 in Table 2 represents 10% slag, 45% fly ash and 45% red mud; the rest of the mixing ratios were similar to this description and will not be repeated. Furthermore, OPC mortar was adopted as the benchmark control group. The experimental process of GPM repair concrete substrate was to first put the silica-aluminate raw materials and fine aggregates together into the mixing pot and stir fully for 3 min to form a uniform mixture. Next, add the preblended alkali activator and tap water in turn and stir evenly again for 3 min to make GPM, and finally pour the GPM into the steel mold with the concrete substrate placed in advance to fully vibrate and scrape. The repaired specimens were demolded after 1 d of curing at room temperature, and then transferred to the standard curing room to continue curing until the predetermined age, after which the mechanical tests were carried out. The experimental procedure for OPC mortar repair of concrete substrate was analogous to that of geopolymer repair mortar and will not be repeated here. It is essential to emphasize that the rough surface of the concrete substrate must be thoroughly cleaned before pouring the repair mortar.

**Table 2.** Mix design of geopolymer mortar.

| Detail | Slag (wt.%) | Fly Ash (wt.%) | Red Mud (wt.%) | OPC (wt.%) | Binder/ Sand | Alkali Activator | | Water/ Binder |
| | | | | | | Modulus | Content (wt.%) | |
|---|---|---|---|---|---|---|---|---|
| S33F33R33 | 33 | 33 | 33 | - | 2 | 1.2 | 40 | 0.4 |
| S10F45R45 | 10 | 45 | 45 | - | 2 | 1.2 | 40 | 0.4 |
| S15F42.5R42.5 | 15 | 42.5 | 42.5 | - | 2 | 1.2 | 40 | 0.4 |
| S20F40R40 | 20 | 40 | 40 | - | 2 | 1.2 | 40 | 0.4 |
| S45F10R45 | 45 | 10 | 45 | - | 2 | 1.2 | 40 | 0.4 |
| S42.5F15R42.5 | 42.5 | 15 | 42.5 | - | 2 | 1.2 | 40 | 0.4 |
| S40F20R40 | 40 | 20 | 40 | - | 2 | 1.2 | 40 | 0.4 |
| S45F45R10 | 45 | 45 | 10 | - | 2 | 1.2 | 40 | 0.4 |
| S42.5F42.5R15 | 42.5 | 42.5 | 15 | - | 2 | 1.2 | 40 | 0.4 |
| S40F40R20 | 40 | 40 | 20 | - | 2 | 1.2 | 40 | 0.4 |
| OPC100 | - | - | - | 100 | 2 | - | - | 0.4 |

*2.4. Testing Method*

Splitting tensile test, double-sided shear test, and three-point bending test were conducted according to ASTM C496-17, JGJ/T70-2009, and ASTM C293-08, respectively, to evaluate the different mechanical characteristics of the bonded interface between the repair mortar and the concrete substrate. The test procedures for the different mechanical properties are shown in Figure 2.

2.4.1. Splitting Tensile Test

As shown in Figure 2a, the splitting tensile test was carried out on a 1000 kN electro-hydraulic servo machine with displacement loading, and the loading rate was controlled at 0.5 mm/min; the test was stopped when the vertical cracks penetrated through the whole section. The dimensions of the concrete substrate and repair mortar used in the test were 150 mm × 150 mm × 75 mm. Three parallel specimens were used for each group test, and the average of the collected results was regarded as the final splitting tensile strength. The splitting tensile strength was calculated according to Equation (1).

$$f_t = \frac{2P_u}{\pi A_t}$$
(1)

where $f_t$ is the splitting tensile strength (MPa), $P_u$ is the maximum load applied at the time of fracture damage (kN), and $A_t$ is the bonded interface area (mm$^2$).

2.4.2. Double-Sided Shear Test

The implementation procedure of the double-sided shear test was referred to in the study of Momayez et al. [51]. The specific experimental procedure is shown in Figure 2b, where centralized loading was achieved by setting up the bedding and ensuring that the lower bedding was in the same vertical plane as the upper bedding during loading; the loading procedure was the same as that for split tensile test. In the double-sided shear test, the dimensions of the concrete substrate were 150 mm × 150 mm × 100 mm, the dimensions of the repair mortar were 150 mm × 150 mm × 50 mm, and the dimensions of the mat were 150 mm × 50 mm × 20 mm. The double-sided shear strength is calculated according to Equation (2).

$$f_s = \frac{P_u}{2A_t} \tag{2}$$

where $f_s$ is the double-sided shear strength (MPa), $P_u$ is the maximum load applied at the time of fracture damage (kN), $A_t$ is the bonded interface area (mm$^2$).

2.4.3. Three-Point Bending Test

The original concrete substrate was first subjected to a three-point bending test to obtain two concrete substrates with the same dimensions to be repaired, and then the fracture surfaces were roughened and cleaned via mechanical chiseling to ensure consistent roughness. As shown in Figure 2c, two concrete substrates to be repaired were placed in a 100 mm × 100 mm × 400 mm steel mold, and then the repair mortar was injected into the fracture surface intersection and fully vibrated, where the width of the repaired cracks was 10 mm~15 mm. The three-point bending test was loaded in the same way as the splitting tensile test, until the specimen was loaded to complete fracture to end the test. The three-point bending strength is calculated according to Equation (3).

$$\sigma_b = \frac{3PL}{2bd^2} \tag{3}$$

where $\sigma_b$ is the three-point bending strength (MPa), $P$ is the maximum load applied at fracture damage (N), $L$ is the base support span (mm), $b$ is the cross-sectional width of the specimen (mm), and $d$ is the cross-sectional height of the specimen (mm).

*2.5. Characterization Methods*

In order to elucidate the mechanism of chemical interaction between GPM and concrete substrate, the microstructural characteristics of the interfacial transition zone (ITZ) were determined by carrying out an SEM test with reference to previous research reports [52–54] on the one hand, and XRD test was undertaken to investigate the mineral crystalline phase composition of GPM to determine the main source of the interfacial bond strength between GPM and concrete substrate on the other hand. The ITZ core fragments and GPM fragments were collected at the end of the double-sided shear test, sealed in anhydrous ethanol for 24 h to terminate the hydration behavior of the silica-aluminate material, and then dried in a desiccator at low temperature to a constant weight. The SEM test was undertaken on a ZEISS Sigma 300 field emission scanning electron microscope, and the implementation procedure was to cut the dried particles into shredded particles with a cross-sectional size of approximately 5 mm, after which they were subjected to an embedding, sanding, and polishing process, followed by evacuation, gold-spraying, and observational analysis. The XRD test was carried out by first mechanically grinding the dried particles into a powder passing a standard sieve of 0.075 mm and then observing and analyzing them on a Rigaku Smart Lab SE fixed-target X-ray powder diffractometer, where the operating conditions had a scanning range of 5°–90° and a scanning speed of 8°/min.

## 3. Results and Discussion

### 3.1. Compressive Strength of Geopolymer Mortar

The compressive strength of the GPM under different silica-alumina raw material ratio conditions is illustrated in Figure 3. Figure 3a depicts the variation of compressive strength of GPM with slag content, and in general the compressive strength of GPM at different curing ages grows approximately linearly and continuously with increasing slag content. The compressive strengths of S10F45R45, S15F42.5R42.5, S20F40R40, and S33F33R33 at a curing age of 28 d were 20.3, 27.7, 35.5 and 67.9 MPa with OPC100 (32.2 MPa) as the reference control group. The strength change rates were −36.96%, −13.98%, 10.25%, and 110.87%, respectively. It can be inferred that the increase in slag content is beneficial to the development of mechanical properties of GPM, which can be mainly attributed to the fact that slag belongs to the category of high calcium system and potentially high activity, which produces calcium-based gel products with early-strength properties after geopolymerization reactions [55].
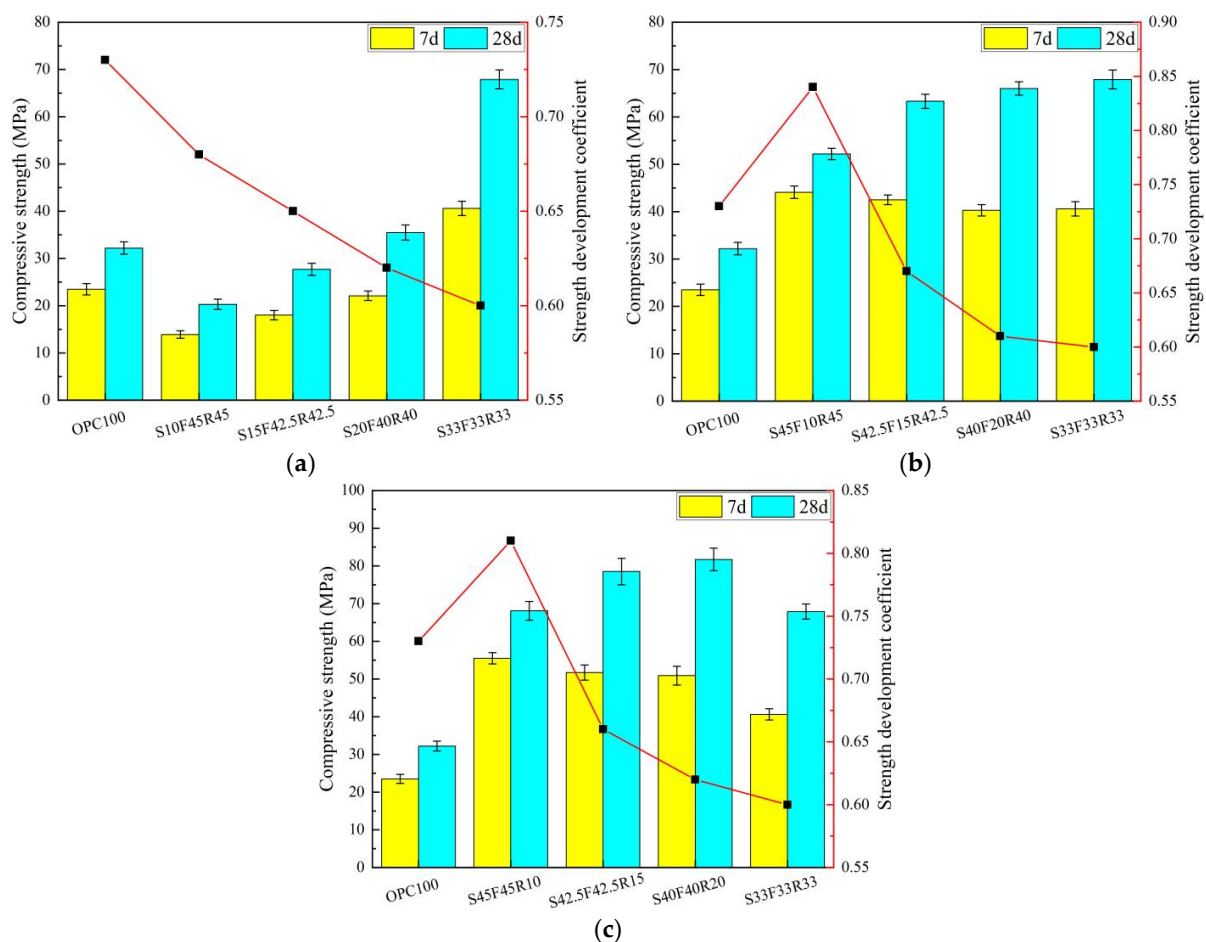


**Figure 3.** The compressive strength of geopolymer repair mortar. (**a**) Slag gradient group, (**b**) fly ash gradient group, and (**c**) red mud gradient group.

Figure 3b describes the trend of the compressive strength of GPM with the content of fly ash, which specifically demonstrated that the compressive strength of GPM gradually grew with the increase in fly ash admixture to the stage of stable and slow change with 15% of fly ash admixture as the cut-off point. The compressive strength of GPM was 63.3 MPa when the fly ash admixture was 15%, and the strength growth rate compared to cement repair mortar was 196.58%. The above results indicated that the incorporation of appropriate amount of fly ash was favorable to the improvement of mechanical properties of GPM, whereas its enhancement effect was not significant after excessive incorporation. The benefi-

cial effects of fly ash were reflected in the enhanced geopolymerization effect and tumbling effect, which can be summarized as, on the one hand, fly ash rich in silica-alumina mineral components can provide more active silica-alumina raw materials, enhance the geopolymerization reaction process, and increase the generation of hydration gel products [56]. Furthermore, fly ash with tumbling form may effectively reinforce the compatibility of GPM system, make the spatial distribution range of geopolymer gel products more fully uniform, and improve the internal pore structure characteristics [57].

From Figure 3c, it can be observed that the compressive strength of GPM showed a trend of gradually increasing and then decreasing with the addition of red mud, in which the compressive strength of GPM under the condition of 20% red mud addition reached the maximum 81.7 MPa, and the strength growth rate was 153.73% compared with that of cement repair mortar. The positive effect of red mud on the mechanical properties of GPM was reflected by the high alkalinity of red mud, which can effectively promote the precursor materials to react more fully and completely with geopolymerization. The high specific surface area of red mud, which can be used as mineral filler to populate the residual pores in the internal structure of the specimen and enhance the structural denseness of the geopolymer [38]. It should not be overlooked that the silica-alumina component of the red mud produced via the Bayer method was less active and required more alkali activator consumption under the same conditions, resulting in a lower effective amount of precursor material subjected to activation [58], which explained why excessive incorporation of red mud led to weakened mechanical behavior of the GPM.

In order to clarify the pattern of change of compressive strength with curing age of GPM under different silica-alumina raw material ratio conditions, the strength development coefficient (the ratio of compressive strength at curing age of 28 d to that at curing age of 7 d) was defined to quantify the variability of strength development of different types of GPM. As presented in Figure 3a, the strength development coefficient of the GPM gradually decreased with the increase in slag admixture, where the strength development coefficients of S10F45R45, S15F42.5R42.5, S20F40R40, and S33F33R33 were 0.68, 0.65, 0.62, and 0.60, respectively. The above results may be attributed to the fact that the increase in slag admixture weakened the positive effect of fly ash and red mud on the geopolymerization reaction of the precursor raw materials. As shown in Figure 3b, the strength development coefficient of GPM decreased significantly and then slowly with the increase in fly ash admixture, which can be explained mainly by the high stability of fly ash itself (particle structure denseness and surface activation energy) weakening the effective amount of alkali activator [59]. In addition, fly ash generates a chemically stable sodium-based gel product N-A-S-H under the activation of alkali activator, which plays an inhibitory role in the generation of calcium-based gel products. As indicated in Figure 3c, the trend of the strength development coefficient of the GPM with the amount of red mud admixture was similar to that of fly ash, which was mainly attributed to the inert nature of the silica-alumina mineral fraction in red mud.

### 3.2. Splitting Tensile Strength

The experimental results of the split tensile test are illustrated in Figure 4. The interfacial bond strength between the repair material and the existing concrete substrate always consists of a combination of physical, chemical, or mechanical effects such as adhesive and van der Waals forces induced by the repair material, frictional resistance generated by rough interfaces, and mechanical interlocking effects between the exposed aggregates [60]. Since the surface roughness of the concrete substrate was uniform in this test, the interfacial bond strength between the GPM and the concrete substrate mainly depended on the bond mechanical properties of the GPM. As can be seen in Figure 4a, the overall split tensile strength of the GPM repaired concrete substrate continued to grow with the increase in slag content within a certain range, but a partial weakening of the split tensile strength occurred when the slag content exceeded 20%. With OPC100 as the reference group, the corresponding growth rates of splitting tensile strength for S10F45R45, S15F42.5R42.5, S20F40R40, and S33F33R33 were −5.0%, 16.3%, 35.6%, and 15.0%, respectively. Unsurprisingly, the reason

that the split tensile strength at 10% slag content was lower than the benchmark group. This was because the calcium content of the active component in the GPM system was simply too low to allow for a reduction in the generation of calcium-based geopolymer gel products, resulting in a lower degree of contribution to the strength of the GPM. However, when the dosage of slag exceeded a certain threshold, the rapid hydration of the active calcium component in the slag induced the enhancement of capillary tension in the internal structure of the geopolymer gel, which enlarged the drying shrinkage of the geopolymer, thus weakening the interfacial adhesion between the GPM and the concrete substrate [7].
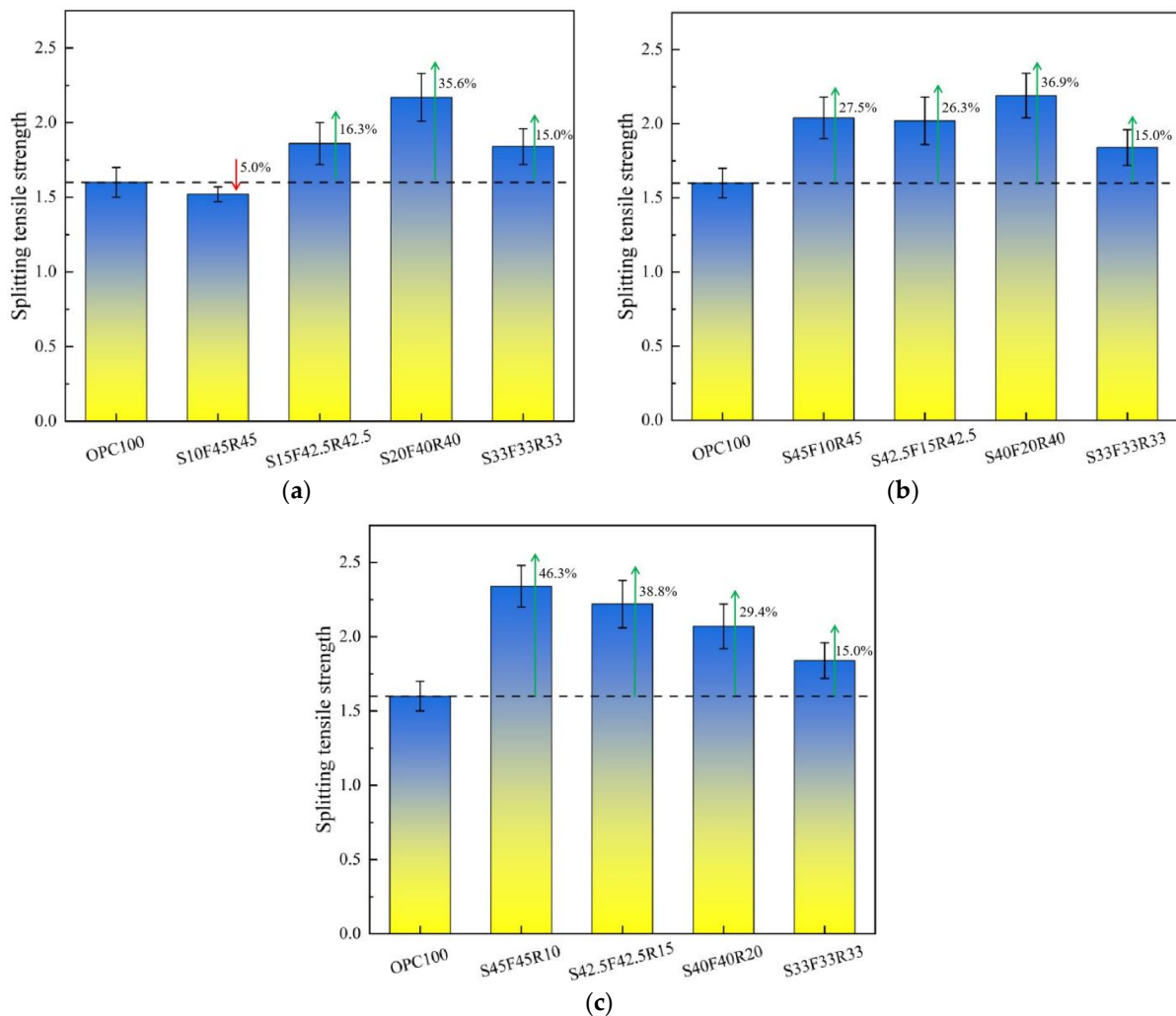


**Figure 4.** The splitting tensile strength of geopolymer mortar and concrete substrate. (**a**) Slag gradient group, (**b**) fly ash gradient group, and (**c**) red mud gradient group.

Figure 4b reveals that the splitting tensile strength of GPM and concrete substrate with different fly ash dosage was relatively higher than that of cement repair mortar under the same dosage condition, which was manifested in the fact that the splitting tensile strength rose continuously and then decreased with the addition of fly ash content. Taking OPC100 as the base group, the growth rates of split tensile strength corresponding to S45F10R45, S42.5F15R42.5, S40F20R40, and S33F33R33 were 31.9%, 34.6%, 44.9%, and 21.3%, respectively. The above results can be attributed to the favorable effects of moderate addition of fly ash in terms of geopolymerization enhancement and tumbling effect, while the unfavorable effects of excessive incorporation of fly ash were in terms of its inhibition of geopolymerization reactions [56,57].

As shown in Figure 4c, unlike the slag and fly ash gradient groups, the increase in red mud content produced a sustained negative effect on the splitting tensile strength of the

GPM repaired concrete substrate. Compared to OPC100, the growth rates of split tensile strength corresponding to S45F45R10, S42.5F42.5R15, S40F40R20, and S33F33R33 were 46.3%, 38.8%, 29.4%, and 15.0%, in that order. From this, it can be judged that red mud with high alkalinity was limited to enhancing the geopolymerization effect on the precursor raw materials, however, the silica-aluminum mineral components in red mud were mostly inert and struggled to participate in the geopolymerization reaction, which disturbed the pore distribution characteristics within the geopolymer restoration mortar and augments the structural porosity [58].

### 3.3. Double-Sided Shear Strength

Figure 5 exhibits the experimental results of GPM-repaired concrete substrate after double-sided shear test. As obtained in Figure 5a, the double-sided shear strength of the bond interface between the GPM and the concrete substrate progressively enhanced with the increase in slag content. The growth rates of double-sided shear strength corresponding to S10F45R45, S15F42.5R42.5, S20F40R40, and S33F33R33 were −3.9%, 46.3%, 13.7%, and 33.3%, respectively, with OPC 100 as the parallel control group. The above phenomenon stemmed from the fact that the increase in slag content promoted the production of calcium-based geopolymer gel products, which generated an "embedding effect" that effectively prevented relative shear slip damage at the interface between the GPM and concrete substrate, thus enhancing the interfacial bond between the GPM and concrete substrate [34].
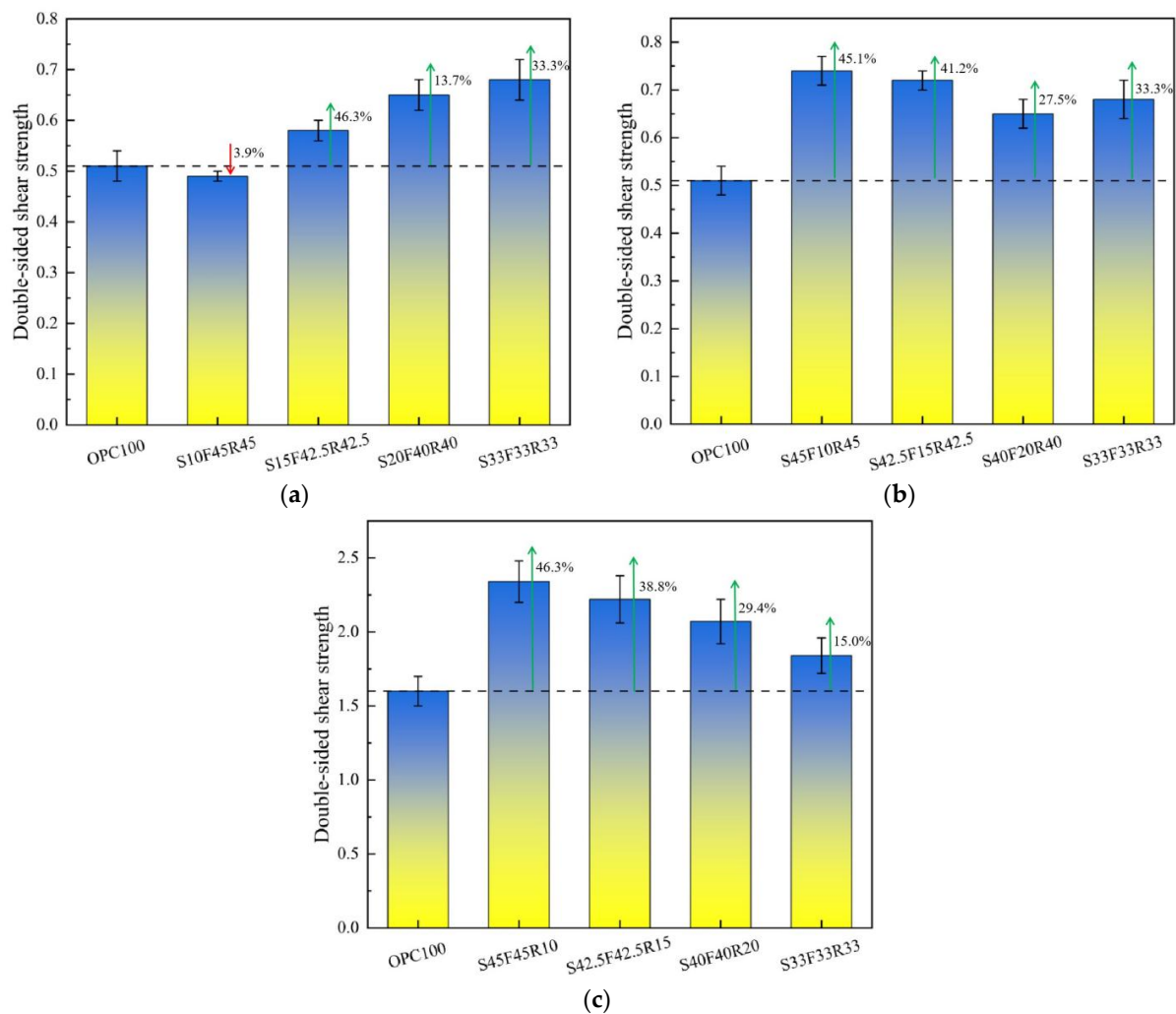


**Figure 5.** The double-sided shear strength of geopolymer mortar and concrete substrate. (**a**) Slag gradient group, (**b**) fly ash gradient group, and (**c**) red mud gradient group.

As shown in Figure 5b, the pattern of change of double-sided shear strength of GPM repaired concrete substrate was negatively correlated with the growth of fly ash content, in other words, the double-sided shear strength continued to decline continuously with the growth of fly ash content. With reference to OPC100, S45F10R45, S42.5F15R42.5, S40F20R40, and S33F33R33 corresponded to double-sided shear strength growth rates of 45.1%, 41.2%, 27.5%, and 33.3%, respectively. It was inferred that the available chemically stable fly ash particles exerted a significant negative effect on the mechanical properties of GPM by inhibiting the geopolymerization reaction process of the precursor raw materials.

Figure 5c demonstrates the developmental pattern of the double-sided shear strength of the GPM-repaired concrete with the growth of the red mud content in agreement with the fly ash. With respect to OPC100, the corresponding double-sided shear strength growth rates for S45F45R10, S42.5F42.5R15, S40F40R20, and S33F33R33 were 46.3%, 38.8%, 29.4%, and 15.0%, respectively. The analysis showed that red mud, which is rich in a substantial amount of inactive silica-aluminum fractions, reduced the proportion of active silica-aluminum fractions in geopolymer, thereby inhibiting the development of the mechanical properties of GPM [58].

### 3.4. Three-Point Bending Strength

The experimental results of GPM-repaired concrete substrate after three-point bending test are presented in Figure 6. As can be seen in Figure 6a, the three-point bending strength of the GPM-repaired concrete substrate increased stepwise with the increase in slag content. Taking OPC100 as the reference group, the corresponding three-point bending strength growth rates for S10F45R45, S15F42.5R42.5, S20F40R40, and S33F33R33 were −18.5%, −15.0%, −21.3%, and 21.3%, respectively. The above results indicated that the three-point bending strength of the GPM repaired concrete substrate was lower than that of the cement repair mortar when the slag content was below a certain amount, which can be attributed to the weaker flexural properties than compressive properties of the calcium-based geopolymer hydration products. This was specifically manifested in the GPM repaired concrete substrate to withstand the external load once more than its interfacial cracking load; the whole was along the destruction of the cracking surface of the continued rapid destruction and the bearing capacity was greatly reduced.

From Figure 6b, it can be obtained that the three-point bending strength of the GPM repaired concrete substrate showed a trend of sustained increase and then decrease with the addition of fly ash content. Compared to OPC100, the corresponding three-point bending strength growth rates for S10F45R45, S15F42.5R42.5, S20F40R40, and S33F33R33 were 31.9%, 34.6%, 44.9%, and 21.3%, respectively. The above phenomena can be explained by the geopolymerization enhancement effect and the tumbling effect contributed by moderate amounts of fly ash leading to an increase in the generation of geopolymer gel products, especially sodium-based hydration products (N-A-S-H), and in this way, facilitating the development of the flexural properties of GPM repaired concrete substrate. The inhibitory effect of geopolymerization exhibited by excessive fly ash played a major role in weakening the load-bearing behavior of the geopolymer mortar-repaired concrete substrate.

Figure 6c depicts the three-point bending strength of GPM-repaired concrete substrate with the increase in red mud content that first decreased continuously. With OPC100 as the reference group, the corresponding three-point bending strength growth rates for S10F45R45, S15F42.5R42.5, S20F40R40, and S33F33R33 were 40.2%, 27.6%, 25.2%, and 21.3%, respectively. The reason for these results was that most of the silica-aluminum mineral components in red mud were inert and not involved in the geopolymerization reaction process, thus reducing the output of geopolymer gel products and significantly weakening the load-bearing properties of the GPM repaired concrete substrate.
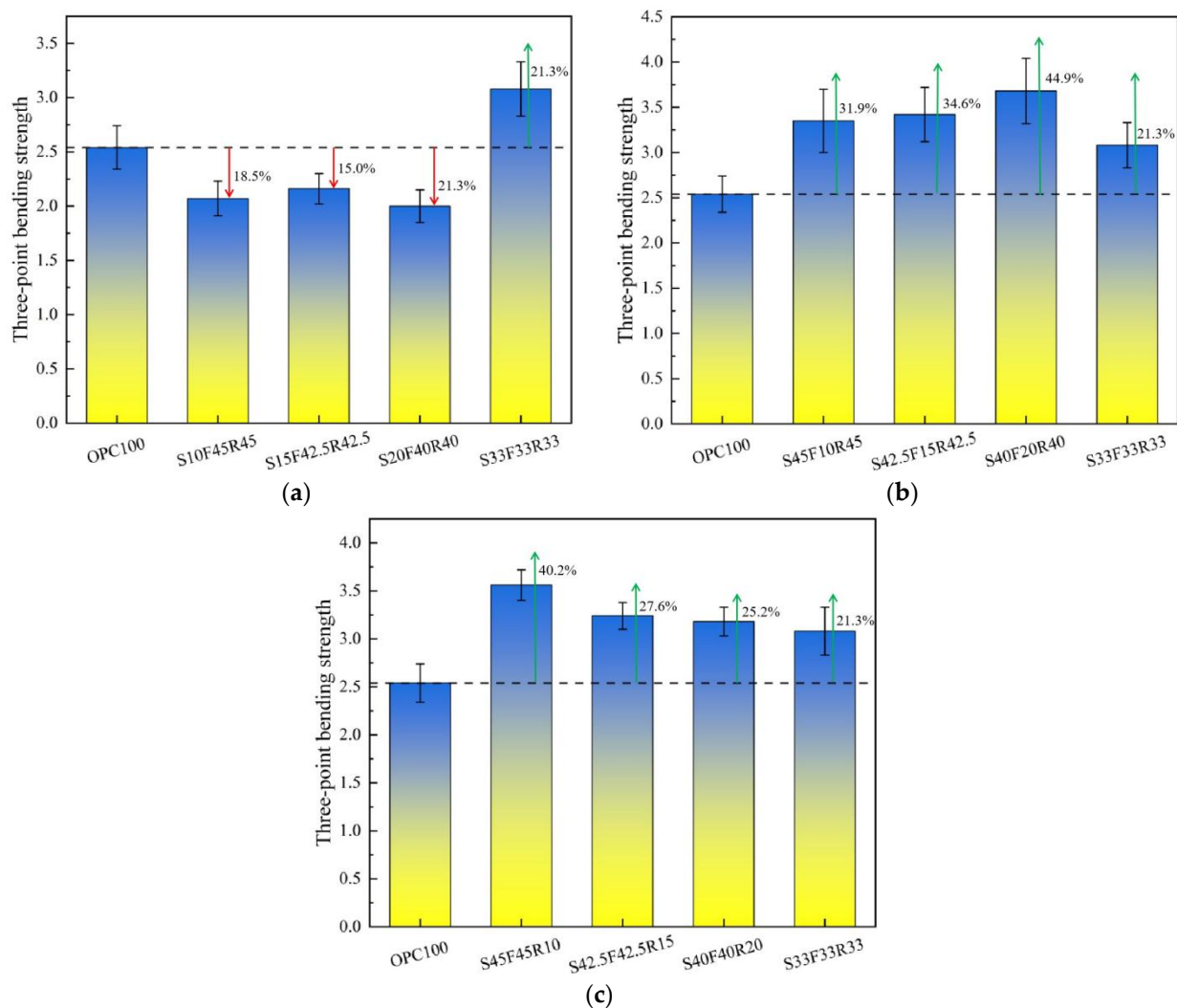
**Figure 6.** The three-point bending strength of geopolymer mortar and concrete substrate. (**a**) Slag gradient group, (**b**) fly ash gradient group, and (**c**) red mud gradient group.

### 3.5. SEM Analysis

In order to further analyze the formation mechanism of the interfacial bond strength of GPM repairing concrete substrate, the specimen in the ITZ, after the double-sided shear test, was selected as the research object, and its microstructural characteristics were analyzed via SEM test. Figure 7a–c show that the GPM with more holes of variable shapes and different distribution ranges at slag dosage not exceeding 15% may be attributed to the evaporation loss of water from the geopolymer gel production during the set-hardening process. In addition to this, what was noticeable was the presence of a high quantity of fly ash and red mud particles not involved in the geopolymerization reaction throughout the interior of the substrate, as well as wide cracks located close to the side of the GPM. The above findings can be interpreted as the low content of highly reactive slag could not induce enough geopolymer gel products to sufficiently bond and encapsulate the fly ash and red mud particles. As the slag content grew to 20%, the number of internal holes shrank significantly, but traces of penetrating microcracks were still found.
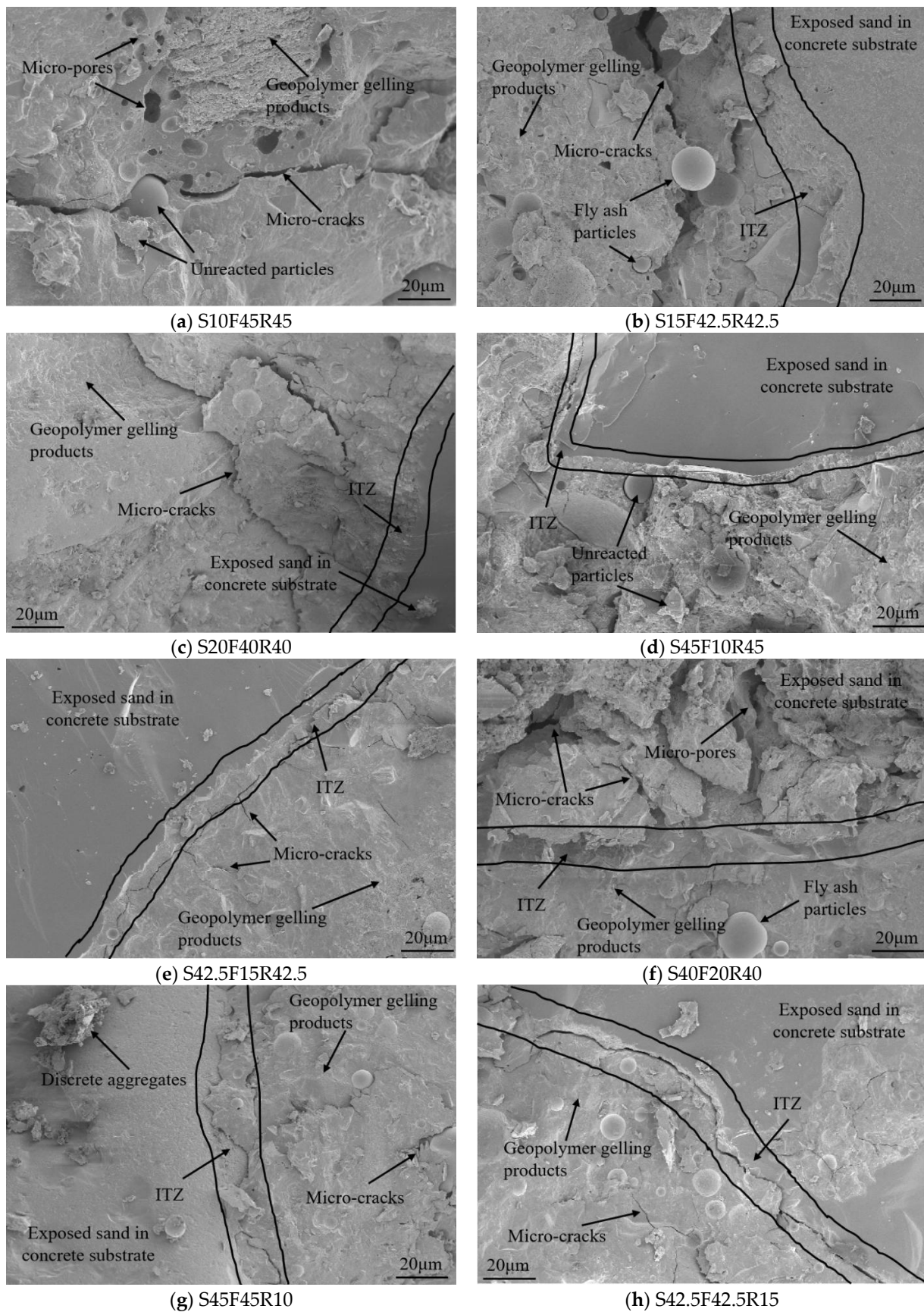
(**a**) S10F45R45

(**b**) S15F42.5R42.5

(**c**) S20F40R40

(**d**) S45F10R45

(**e**) S42.5F15R42.5

(**f**) S40F20R40

(**g**) S45F45R10

(**h**) S42.5F42.5R15

**Figure 7.** *Cont*.

(i) S40F40R20
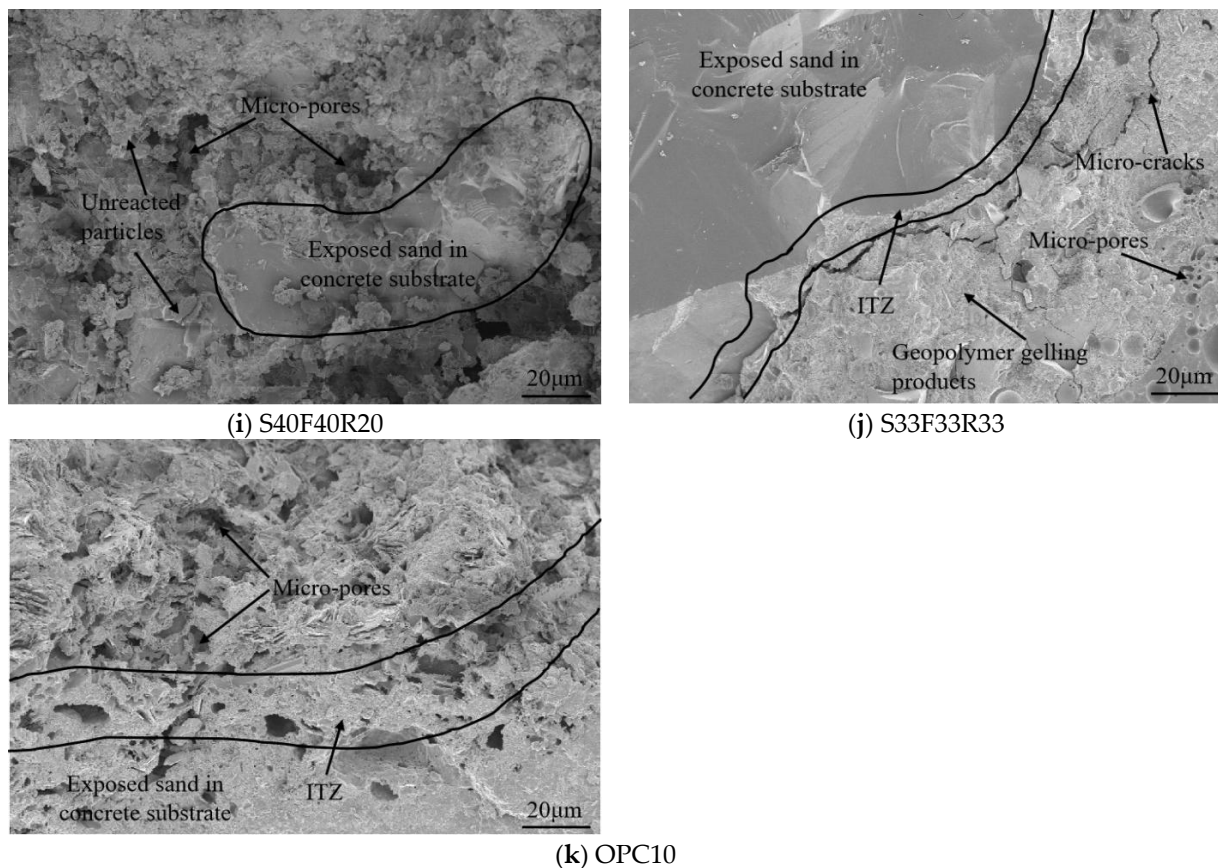


(j) S33F33R33



(k) OPC10

**Figure 7.** The SEM images of ITZ of geopolymer mortar with concrete substrate.

As can be seen in Figure 7d–f, the geopolymer gel products were significantly increased and the overall densification of the internal spatial structure was enhanced due to the geopolymerization enhancement effect and the ballooning effect provided by the fly ash at a dosage of less than 15%. The above results were specifically demonstrated by the fact that the ITZ between the GPM and the concrete substrate exhibited a complete continuity. However, as the fly ash content was raised to 20%, a limited proportion of unreacted fly ash particles gradually appeared in the internal structure. On the other hand, there was a clear boundary between the GPM and the concrete substrate accompanied by obvious microcracks, in which the structure on the side near the concrete substrate was loose and porous. It can be concluded that excessive fly ash is detrimental to the development of the mechanical properties of GPM, resulting in a weakening of the interfacial bond to the concrete substrate.

From Figure 7g–i, it can be concluded that the red mud dosed with no more than 15% can give considerable alkalinity and physical filling effect, which makes the increasing geopolymer gel products stacked with each other, and effectively enhances the degree of structural densification. However, it was still convenient to discover some flaky adherents on the surface of the GPM substrate and microcracks in the ITZ between the geopolymer mortar and the concrete substrate. When the red mud dosage was increased to 20%, the distribution of attachments on the GPM and concrete substrate was further expanded, and the surface roughness was increased, accompanied by clearly visible pore defects. This may stem from the fact that the inert silica-aluminum mineral fraction present in the red mud did not participate in the geopolymerization reaction and only acted as a filler for the mineral particles, resulting in a significant reduction in the yield of geopolymer gels.

Figure 7j suggests that under the condition of slag, fly ash, and red mud mixed in equal proportions, the precursor raw materials were able to generate sufficient geopolymer cementation products under the effect of excitation and activation, which possessed better

mechanical bonding properties, making the ITZ between the GPM and the concrete substrate continuous and intact. However, it need to be clarified that a minority of microcracks still existed within the structure. Figure 7k reveals that compared to the GPM, the internal structure of the cement mortar was discrete and loose, with a large distribution of porous defects, which may be attributed to the random uncontrolled evaporation of water and the negative effect of self-shrinkage during the set-hardening process of the cement mortar. In addition, there were obvious cracks between the cement mortar and the concrete substrate, and the overall joint over performance was weakened, which was macroscopically manifested as a significant attenuation of the interfacial bond strength of the cement mortar repairing the concrete substrate.

### 3.6. XRD Analysis

The XRD test was carried out to investigate the physical composition of different types of GPM. The results of XRD profiles of GPM with different slag, fly ash, and red mud mixing ratios are presented in Figure 8. Figure 8a–c exhibit that the mineral composition of each type of GPM belonged to a mixed composition of crystalline and amorphous phases. The crystalline phases of the mineral composition can be summarized as quartz, calcite, and hematite, with quartz being largely derived from the fine aggregates and precursor raw materials used in the preparation of the mortar, which were classified as inert and did not take part in the geopolymerization hydration reactions; they had no influence on the evolution of the generation of the geopolymer hydration gels. The formation of calcite may be attributed to the carbonation of calcium-based hydration products by combining free carbon dioxide and moisture in the air during standard maintenance at the end of preparation. The presence of hematite can be interpreted as the red mud prepared via the Bayer method that contained a portion of $Fe_2O_3$ in the form of crystals, which were chemically stable and did not participate in geopolymer hydration reactions. The above results show again that the influence of hematite on the crystalline phase of the minerals in GPM was mainly due to its high alkalinity, which led to an increase in the alkalinity of the reaction system, thus intensifying the evolution of the geopolymerization of the precursor raw materials and increasing the number of different types of geopolymer gel products.

From Figure 8a, it can be analyzed that the intensity of the diffraction peaks of the calcium-based hydration products (C-S-H, C-A-S-H), which determined the development of the mechanical properties in GPM, were subsequently enhanced with the growth of the slag content. This suggested that slag held a relatively strong potential reactivity to preferentially bind alkali activator and underwent geopolymerization under equal conditions, generating calcium-based hydration products that promoted the development of interfacial bond strength between GPM and concrete substrates. The above findings remain in agreement with the pattern of change in the macroscopic mechanical properties of GPM with slag content.

Figure 8b demonstrates that the improvement in fly ash content heightened the production of sodium-based hydration products (N-A-S-H), but at the same time it suppressed the development of different types of calcium-based hydration products. This can be accounted for by the fact that the reactive mineral fraction enriched in fly ash combined with the $Na^+$ in the alkali activator in a geopolymerization to form N-A-S-H. However, the sodium-based hydration products were particularly chemically stable and structurally solid and cannot react with the calcium-based hydration products in secondary reactions, resulting in a significant reduction in the effective amount of calcium-based hydration products in GPM. At the same time, the mechanical properties of sodium-based hydration products were weaker compared to those of calcium-based hydration products, which under these conditions weakened the development of mechanical properties of GPM.

It can be inferred from Figure 8c that the inclusion of red mud facilitates the expansion of calcium- and sodium-based hydration products within a certain range, but once the optimal amount of inclusion was exceeded, red mud played more of a negative role. The above results indicated that with the increase in red mud doping, the positive effect of

alkalinity provided by red mud itself was gradually weakened, while the consumption of inert silica-aluminum components for alkaline activator was constantly rising, resulting in the reduction in the effective activator in the reaction system; the red mud showed more negative effects on the geopolymerization. The above-mentioned results were in agreement with the outcomes of the macromechanical tests, and the addition of excessive fly ash and red mud was rather detrimental to the subsequent development of the interfacial bond strength between the GPM and the concrete substrate. The categories of hydration gel products in the cement mortar in Figure 8d are mainly C-S-H and C-A-H, which were in accordance with the results of previous investigations [52–54] on the subject and will not be discussed in detail here.
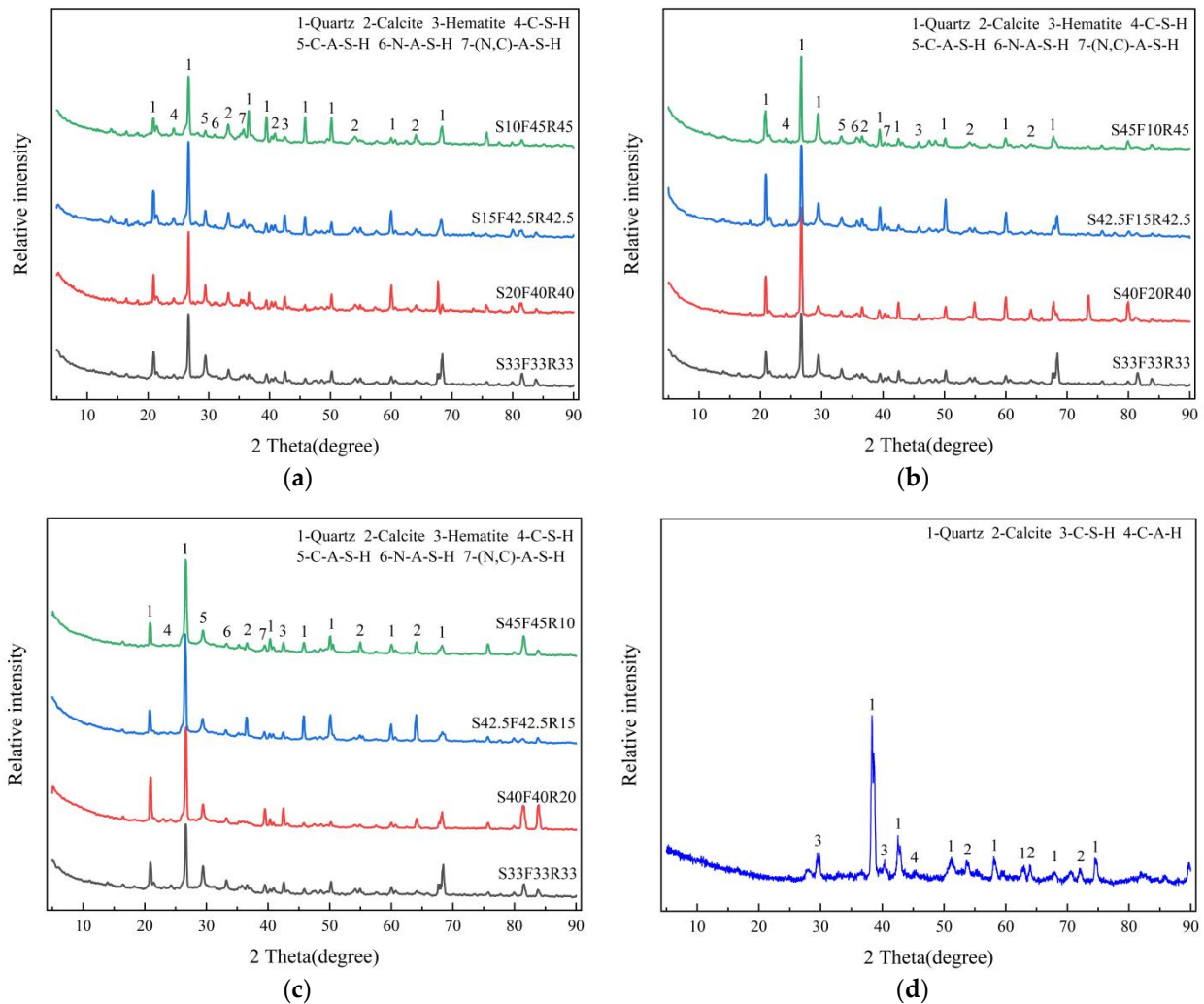


**Figure 8.** The XRD images of geopolymer repair mortar. (**a**) Slag gradient group, (**b**) fly ash gradient group, (**c**) red clay gradient group, and (**d**) cement group.

## 4. Conclusions

The objective of this investigation was to illustrate the influence of different slag, fly ash, and red mud mixing ratio conditions on the interfacial properties of GPM and OPC concrete substrate. On this basis, the interfacial bonding properties of GPM and concrete substrate were investigated by carrying out a split tensile test, a double-sided shear test, and a three-point bending test, as well as microscopic characterization means, such as SEM and XRD. Combined with the experimental results of this study, the following conclusions were drawn:

1.  The compressive strength of the GPM displayed an increasing evolution with the improvement of the slag content, however, with the growth of the fly ash content it revealed a minor increase followed by a gradual levelling off. Limited amounts of red mud produced favorable effects on the compressive strength of GPM to a certain extent, whereas excessive amounts of red mud produced more of a negative effect. Overall, the optimum mix ratio for GPM was S33F33R33 based on compressive strength.
2.  The splitting tensile strength of GPM and concrete substrate with the growth of slag and fly ash content all demonstrated the rule of change of the first growth and then decline, in which the fly ash presented a favorable effect and was better than the slag, however, with the increase in red mud content, it presented an approximate linear decline in the trend of change.
3.  The double-sided shear strength of GPM and concrete substrate exhibited a continuous improvement with the increase in slag content, however, it tended to decrease slowly with the increase in fly ash and red mud content.
4.  The three-point bending strength of GPM and concrete substrate was not as good as that of cement mortar under the condition of less slag mixing, however, with the increase in fly ash content, it presented the variation tendency of increasing and then decreasing, and with the growth of red mud content, exhibited a continuous decreasing trend.
5.  From the SEM analysis, it can be seen that the number and distribution range of pores and microcracks in the ITZ of GPM and concrete substrate gradually shrank with the increase in slag dosage. Under the condition of moderate amount of fly ash, the ITZ of GPM and concrete substrate exhibited complete and considerable continuity, however, the higher content of fly ash caused microcracks to appear in the ITZ, and the internal structure of the GPM showed the characteristics of being loose and porous. An appropriate quantity of red mud can effectively improve the structural density of GPM and enhance the smooth continuity of ITZ, but excessive red mud leads to the increase in surface roughness and the generation of porous defects in ITZ.

**Author Contributions:** Conceptualization, Q.L., Y.Z. and B.Z.; Investigation, H.Y., Z.L. (Zhengdong Luo), Z.L. (Zhengyang Li), G.Z. and K.L.; Writing-original draft preparation, H.Y., Z.L. (Zhengdong Luo), Z.L. (Zhengyang Li), G.Z. and K.L.; Writing-review and editing, Q.L., Y.Z. and B.Z. All authors have read and agreed to the published version of the manuscript.

**Data Availability Statement:** The data used to support the results of this study are available from the corresponding author upon reasonable request.

**Conflicts of Interest:** Author Qinghui Long was employed by Yiyang Highway and Bridge Construction Co., Ltd., China, and Kun Liu was employed by Hunan Zhitong Expressway Construction and Development Co., Ltd., China. The remaining authors declare that the research was conducted in the absence of any commercial or financial relationships that could be construed as a potential conflict of interest.

## References

1.  Masoud, M.A.; Kansouh, W.A.; Shahien, M.G.; Sakr, K.; Rashad, A.M.; Zayed, A.M. An experimental investigation on the effects of barite/hematite on the radiation shielding properties of serpentine concretes. *Prog. Nucl. Energ.* **2020**, *120*, 103220. [CrossRef]
2.  Zayed, A.M.; Masoud, M.A.; Rashad, A.M.; El-Khayatt, A.M.; Sakr, K.; Kansouh, W.A.; Shahien, M.G. Influence of heavyweight aggregates on the physico-mechanical and radiation attenuation properties of serpentine-based concrete. *Constr. Build. Mater.* **2020**, *260*, 120473. [CrossRef]

3.  Masoud, M.A.; El-Khayatt, A.M.; Kansouh, W.A.; Sakr, K.; Shahien, M.G.; Zayed, A.M. Insights into the effect of the mineralogical composition of serpentine aggregates on the radiation attenuation properties of their concretes. *Constr. Build. Mater.* **2020**, *263*, 120141. [CrossRef]

4.  Rodrigues, R.; Gaboreau, S.; Gance, J.; Ignatiadis, I.; Betelu, S. Reinforced concrete structures: A review of corrosion mechanisms and advances in electrical methods for corrosion monitoring. *Constr. Build. Mater.* **2021**, *269*, 121240. [CrossRef]

5.  Peng, L.; Zeng, W.; Zhao, Y.; Li, L.; Poon, C.; Zheng, H. Steel corrosion and corrosion-induced cracking in reinforced concrete with carbonated recycled aggregate. *Cem. Concr. Compos.* **2022**, *133*, 104694. [CrossRef]

6.  Tian, Y.; Zhang, G.; Ye, H.; Zeng, Q.; Zhang, Z.; Tian, Z.; Jin, N.; Jin, N.; Chen, Z.; Wang, J. Corrosion of steel rebar in concrete induced by chloride ions under natural environments. *Constr. Build. Mater.* **2023**, *369*, 130504. [CrossRef]

7.  Gomaa, E.; Gheni, A.; ElGawady, M.A. Repair of ordinary Portland cement concrete using ambient-cured alkali-activated concrete: Interfacial behavior. *Cem. Concr. Res.* **2020**, *129*, 105968. [CrossRef]

8.  Liu, D.; Wang, C.; Gonzalez-Libreros, J.; Guo, T.; Cao, J.; Tu, Y.; Elfgren, L.; Sas, G. A review of concrete properties under the combined effect of fatigue and corrosion from a material perspective. *Constr. Build. Mater.* **2023**, *369*, 130489. [CrossRef]

9.  Wang, L.; Zhang, Q. Investigation on water absorption in concrete after subjected to compressive fatigue loading. *Constr. Build. Mater.* **2021**, *299*, 123897. [CrossRef]

10. Wang, P.; Mo, R.; Li, S.; Xu, J.; Jin, Z.; Zhao, T.; Wang, D. A chemo-damage-transport model for chloride ions diffusion in cement-based materials: Combined effects of sulfate attack and temperature. *Constr. Build. Mater.* **2021**, *288*, 123121. [CrossRef]

11. Ukpata, J.O.; Basheer, P.A.M.; Black, L. Slag hydration and chloride binding in slag cements exposed to a combined chloride-sulphate solution. *Constr. Build. Mater.* **2019**, *195*, 238–248. [CrossRef]

12. Shaheen, F.; Pradhan, B. Influence of sulfate ion and associated cation type on steel reinforcement corrosion in concrete powder aqueous solution in the presence of chloride ions. *Cem. Concr. Res.* **2017**, *91*, 73–86. [CrossRef]

13. Wu, L.; Farzadnia, N.; Shi, C.; Zhang, Z.; Wang, H. Autogenous shrinkage of high performance concrete: A review. *Constr. Build. Mater.* **2017**, *149*, 62–75. [CrossRef]

14. Mao, Y.; Liu, J.; Shi, C. Autogenous shrinkage and drying shrinkage of recycled aggregate concrete: A review. *J. Clean. Prod.* **2021**, *295*, 126435. [CrossRef]

15. Woźniak, Z.Z.; Chajec, A.; Sadowski, Ł. Effect of the Partial Replacement of Cement with Waste Granite Powder on the Properties of Fresh and Hardened Mortars for Masonry Applications. *Materials* **2022**, *15*, 9066. [CrossRef] [PubMed]

16. Teixeira, O.G.; Geraldo, R.H.; da Silva, F.G.; Gonçalves, J.P.; Camarini, G. Mortar type influence on mechanical performance of repaired reinforced concrete beams. *Constr. Build. Mater.* **2019**, *217*, 372–383. [CrossRef]

17. Assaad, J.J.; Khayat, K.H. Form pressure characteristics of self-consolidating concrete used in repair. *Cem. Concr. Compos.* **2021**, *122*, 104118. [CrossRef]

18. Reggia, A.; Morbi, A.; Plizzari, G.A. Experimental study of a reinforced concrete bridge pier strengthened with HPFRC jacketing. *Eng. Struct.* **2020**, *210*, 110355. [CrossRef]

19. Valikhani, A.; Jahromi, A.J.; Mantawy, I.M.; Azizinamini, A. Experimental evaluation of concrete-to-UHPC bond strength with correlation to surface roughness for repair application. *Constr. Build. Mater.* **2020**, *238*, 117753. [CrossRef]

20. Gao, T.; Shen, L.; Shen, M.; Chen, F.; Liu, L.; Gao, L. Analysis on differences of carbon dioxide emission from cement production and their major determinants. *J. Clean. Prod.* **2015**, *103*, 160–170. [CrossRef]

21. El-Hassan, H.; Elkholy, S. Enhancing the performance of Alkali-Activated Slag-Fly ash blended concrete through hybrid steel fiber reinforcement. *Constr. Build. Mater.* **2021**, *311*, 125313. [CrossRef]

22. Thomas, B.S.; Yang, J.; Bahurudeen, A.; Chinnu, S.N.; Abdalla, J.A.; Hawileh, R.A.; Hamada, H.M. Geopolymer concrete incorporating recycled aggregates: A comprehensive review. *Constr. Build. Mater.* **2022**, *3*, 100056.

23. Singh, B.; Ishwarya, G.; Gupta, M.; Bhattacharyya, S.K. Geopolymer concrete: A review of some recent developments. *Constr. Build. Mater.* **2015**, *85*, 78–90. [CrossRef]

24. Habert, G.; Miller, S.A.; John, V.M.; Provis, J.L.; Favier, A.; Horvath, A.; Scrivener, K.L. Environmental impacts and decarbonization strategies in the cement and concrete industries. *Nat. Rev. Earth Environ.* **2020**, *1*, 559–573. [CrossRef]

25. Cong, P.; Cheng, Y. Advances in geopolymer materials: A comprehensive review. *J. Traffic Transp. Eng.* **2021**, *8*, 283–314. [CrossRef]

26. Huang, W.; Wang, H. Geopolymer pervious concrete modified with granulated blast furnace slag: Microscale characterization and mechanical strength. *J. Clean. Prod.* **2021**, *328*, 129469. [CrossRef]

27. Nath, P.; Sarker, P.K. Flexural strength and elastic modulus of ambient-cured blended low-calcium fly ash geopolymer concrete. *Constr. Build. Mater.* **2017**, *130*, 22–31. [CrossRef]

28. Albidah, A.; Alghannam, M.; Abbas, H.; Almusallam, T.; Al-Salloum, Y. Characteristics of metakaolin-based geopolymer concrete for different mix design parameters. *J. Mater. Res. Technol.* **2021**, *10*, 84–98. [CrossRef]

29. Bature, A.S.; Khorami, M.; Ganjian, E.; Tyrer, M. Influence of alkali activator type and proportion on strength performance of calcined clay geopolymer mortar. *Constr. Build. Mater.* **2021**, *267*, 120446. [CrossRef]

30. Demir, F.; Derun, E.M. Modelling and optimization of gold mine tailings based geopolymer by using response surface method and its application in $Pb^{2+}$ removal. *J. Clean. Prod.* **2019**, *237*, 117766. [CrossRef]

31. Qaidi, S.M.A.; Tayeh, B.A.; Zeyad, A.M.; de Azevedo, A.R.G.; Ahmed, H.U.; Emad, W. Recycling of mine tailings for the geopolymers production: A systematic review. *Case Stud. Constr. Mat.* **2022**, *16*, e00933. [CrossRef]

32. Laskar, S.M.; Talukdar, S. A study on the performance of damaged RC members repaired using ultra-fine slag based geopolymer mortar. *Constr. Build. Mater.* **2019**, *217*, 216–225. [CrossRef]

33. Zailani, W.W.A.; Abdullah, M.M.A.B.; Arshad, M.F.; Razak, R.F.; Tahir, M.F.M.; Zainol, R.R.M.A.; Nabialek, M.; Sandu, A.V.; Wyslocki, J.J.; Bloch, K. Characterisation at the bonding zone between fly ash based geopolymer repair materials (GRM) and ordinary portland cement concrete (OPCC). *Materials* **2020**, *14*, 56. [CrossRef]

34. Wang, Y.S.; Peng, K.D.; Alrefaei, Y.; Dai, J. The bond between geopolymer repair mortars and OPC concrete substrate: Strength and microscopic interactions. *Cem. Concr. Compos.* **2021**, *119*, 103991. [CrossRef]

35. Wang, S.; Jin, H.; Deng, Y.; Xiao, Y. Comprehensive utilization status of red mud in China: A critical review. *J. Clean. Prod.* **2021**, *289*, 125136. [CrossRef]

36. Zhao, H.; Gou, H. Unfired bricks prepared with red mud and calcium sulfoaluminate cement: Properties and environmental impact. *J. Build. Eng.* **2021**, *38*, 102238. [CrossRef]

37. Mudgal, M.; Singh, A.; Chouhan, R.K.; Acharya, A.; Srivastava, A.K. Fly ash red mud geopolymer with improved mechanical strength. *Clean. Eng. Technol.* **2021**, *4*, 100215. [CrossRef]

38. Khairul, M.A.; Zanganeh, J.; Moghtaderi, B. The composition, recycling and utilisation of Bayer red mud. *Resour. Conserv. Recy.* **2019**, *141*, 483–498. [CrossRef]

39. Atan, E.; Sutcu, M.; Cam, A.S. Combined effects of bayer process bauxite waste (red mud) and agricultural waste on technological properties of fired clay bricks. *J. Build. Eng.* **2021**, *43*, 103194. [CrossRef]

40. Kim, S.Y.; Jun, Y.; Jeon, D.; Oh, J.E. Synthesis of structural binder for red brick production based on red mud and fly ash activated using Ca(OH)$_2$ and Na$_2$CO$_3$. *Constr. Build. Mater.* **2017**, *147*, 101–116. [CrossRef]

41. Xu, X.; Song, J.; Li, Y.; Wu, J.; Liu, X.; Zhang, C. The microstructure and properties of ceramic tiles from solid wastes of Bayer red muds. *Constr. Build. Mater.* **2019**, *212*, 266–274. [CrossRef]

42. Qaidi, S.M.A.; Tayeh, B.A.; Ahmed, H.U.; Emad, W. A review of the sustainable utilisation of red mud and fly ash for the production of geopolymer composites. *Constr. Build. Mater.* **2022**, *350*, 128892. [CrossRef]

43. Zakira, U.; Zheng, K.; Xie, N.; Birgisson, B. Development of high-strength geopolymers from red mud and blast furnace slag. *J. Clean. Prod.* **2023**, *383*, 135439. [CrossRef]

44. Liang, X.; Ji, Y. Experimental study on durability of red mud-blast furnace slag geopolymer mortar. *Constr. Build. Mater.* **2021**, *267*, 120942. [CrossRef]

45. Hertel, T.; Pontikes, Y. Geopolymers, inorganic polymers, alkali-activated materials and hybrid binders from bauxite residue (red mud)-Putting things in perspective. *J. Clean. Prod.* **2020**, *258*, 120610. [CrossRef]

46. Hai, R.; Zheng, J.; Li, J.; Hui, C.; Liu, J. Preparation mechanism and properties of thermal activated red mud and its geopolymer repair mortar. *Case Stud. Constr. Mat.* **2024**, *20*, e02853. [CrossRef]

47. Amran, M.; Debbarma, S.; Ozbakkaloglu, T. Fly ash-based eco-friendly geopolymer concrete: A critical review of the long-term durability properties. *Constr. Build. Mater.* **2021**, *270*, 121857. [CrossRef]

48. Guo, S.; Wu, Y.; Jia, Z.; Qi, X.; Wang, W. Sodium-based activators in alkali-activated materials: Classification and comparison. *J. Build. Eng.* **2023**, *70*, 106397. [CrossRef]

49. Luo, Z.; Zhang, B.; Zou, J.; Luo, B. Sulfate erosion resistance of slag-fly ash based geopolymer stabilized soft soil under semi-immersion condition. *Case Stud. Constr. Mat.* **2022**, *17*, e01506. [CrossRef]

50. Santos, P.M.D.; Julio, E.N.B.S. Correlation between concrete-to-concrete bond strength and the roughness of the substrate surface. *Constr. Build. Mater.* **2007**, *21*, 1688–1695. [CrossRef]

51. Momayez, A.; Ehsani, M.R.; Ramezanianpour, A.A.; Rajaie, H. Comparison of methods for evaluating bond strength between concrete substrate and repair materials. *Cem. Concr. Res.* **2005**, *35*, 748–757. [CrossRef]

52. Zayed, A.M.; Masoud, M.A.; Shahien, M.G.; Gökçe, H.S.; Sakr, K.; Kansouh, W.A.; El-Khayatt, A.M. Physical, mechanical, and radiation attenuation properties of serpentine concrete containing boric acid. *Constr. Build. Mater.* **2021**, *272*, 121641. [CrossRef]

53. Masoud, M.A.; Rashad, A.M.; Sakr, K.; Shahien, M.G.; Zayed, A.M. Possibility of using different types of Egyptian serpentine as fine and coarse aggregates for concrete production. *Mater. Struct.* **2020**, *53*, 1–17. [CrossRef]

54. Masoud, M.A.; El-Khayatt, A.M.; Mahmoud, K.A.; Rashad, A.M.; Shahien, M.G.; Bakhit, B.R.; Zayed, A.M. Valorization of hazardous chrysotile by H$_3$BO$_3$ incorporation to produce an innovative eco-friendly radiation shielding concrete: Implications on physico-mechanical, hydration, microstructural, and shielding properties. *Cem. Concr. Comp.* **2023**, *141*, 105120. [CrossRef]

55. Moudio, A.M.N.; Tchakoute, H.K.; Ngnintedem, D.L.V.; Andreola, F.; Kamseu, E.; Nanseu-Njiki, C.P.; Leonelli, C.; Rüscher, C.H. Influence of the synthetic calcium aluminate hydrate and the mixture of calcium aluminate and silicate hydrates on the compressive strengths and the microstructure of metakaolin-based geopolymer cements. *Mater. Chem. Phys.* **2021**, *264*, 124459. [CrossRef]

56. Luo, Z.; Zhang, B. Effect of humic acid and fulvic acid on mechanical and durability properties of geopolymer stabilized soft soil. *Constr. Build. Mater.* **2023**, *409*, 133875. [CrossRef]

57. Nath, P.; Sarker, P.K. Effect of GGBFS on setting, workability and early strength properties of fly ash geopolymer concrete cured in ambient condition. *Constr. Build. Mater.* **2014**, *66*, 163–171. [CrossRef]

58. Hu, W.; Nie, Q.; Huang, B.; Shu, X.; He, Q. Mechanical and microstructural characterization of geopolymers derived from red mud and fly ashes. *J. Clean. Prod.* **2018**, *186*, 799–806. [CrossRef]

59. John, S.K.; Nadir, Y.; Girija, K. Effect of source materials, additives on the mechanical properties and durability of fly ash and fly ash-slag geopolymer mortar: A review. *Constr. Build. Mater.* **2021**, *280*, 122443. [CrossRef]
60. He, Y.; Zhang, X.; Hooton, R.D.; Zhang, X. Effects of interface roughness and interface adhesion on new-to-old concrete bonding. *Constr. Build. Mater.* **2017**, *151*, 582–590. [CrossRef]